RC131 Amer Zakaria, Ian Jeffrey, Majid Ostadrahimi, Mohammad Asefi, Joe LoVetri (2013) A Novel 3D Near-f ield Microwave Imaging System, 2013 IEEE Int. Symp. on Ant. and Prop. and USNC-URSI National Radio Science Meeting, Orlando, FL, USA, July 7-13, 2013.

A Novel 3D Near-field Microwave Imaging System

Amer Zakaria, Ian Jeffrey, Majid Ostadrahimi, Mohammad Asefi and Joe LoVetri
Electrical and Computer Engineering Department
University of Manitoba
Winnipeg, Manitoba, Canada
Email: Joe_LoVetri@umanitoba.ca

***Abstract*—Preliminary imaging results are shown using datasets collected by a novel three-dimensional microwave imaging system based on the modulated scattering technique. Probes are used to measure the $\phi-$ and $z-$ electric field components at the receivers. Data collected for two objects-of-interest are inverted using the contrast source inversion algorithm formulated using the finite-element method for 3D full-vectorial problems.**

I. Introduction

Microwave imaging (MWI) is a modality in which one attempts to estimate the unknown electrical properties of an object-of-interest (OI), as well as reconstruct the OI's shape and location. Most MWI systems reported in literature collect a single component of the electric field, which only enables inversion algorithms to produce feasibly two-dimensional (2D) reconstructions of an OI profile. Nevertheless, few systems measure several field components that makes it possible to obtain three-dimensional (3D) reconstructions of an OI [1].

In this paper, a novel 3D MWI based on the modulated scattering technique is introduced [2]. The datasets collected using the system are inverted using the contrast source inversion (CSI) technique formulated using the finite-element method (FEM) [3].

II. Microwave Imaging System

The MWI system consists of three layers separated by 6.1 cm. The center layer consists of 12 cavity-backed Vivaldi antennas evenly distributed on a circle of 11.5 cm radius from the center of an Plexiglas chamber [2], [4]. These antennas are used as the system's transmitters and collectors. A pair of probes, acting as receivers, is mounted in front of each transmitter; thus the central layer contains 12 probe-pairs. As for the upper and lower layers, each consists of 24 pairs of probes equally spaced on a circle of 9.75 cm radius. Each probe-pair has a probe to measure the $\phi-$component and a probe to measure the $z-$component of the field at the receiver location [2]. Thus, the number of measurement points for each dataset at a single frequency is $12 \times 60 \times 2 = 1440$. An overall picture of the MWI system with a target is shown in Figure 1.

For the purpose of calibrating the measurements for the different OIs, two datasets are collected: (*i*) measurements in the absence of any object inside the imaging chamber, which are referred to as incident field measurements, and (*ii*) measurements in the presence of the a reference object, which was a metallic sphere of 3.75 cm radius. After collecting the dataset for a given OI, the measurements are calibrated using the procedure outlined in [2].

III. Inversion Algorithm

The CSI method is a state-of-the-art technique that formulates the optimization problem in terms of two variables, the contrast source, $\vec{w}_t$ and the contrast, χ [3], [5]. Within the framework of FEM, the discretization of the CSI functional results in the following cost functional over discrete vectors of unknowns:

$$\mathcal{F}^{\text{CSI}}(\underline{\chi}, \underline{\vec{w}}_t) = \frac{\sum_t \left\| \underline{\vec{E}}_t^{\text{sct,meas}} - \vec{\boldsymbol{\mathcal{M}}}_{\mathcal{S}} \vec{\boldsymbol{\mathcal{L}}} [\underline{\vec{w}}_t] \right\|_{\mathcal{S}}^2}{\sum_t \left\| \underline{\vec{E}}_t^{\text{sct,meas}} \right\|_{\mathcal{S}}^2} + \frac{\sum_t \left\| \underline{\chi} \odot \underline{\vec{E}}_t^{\text{inc}} - \underline{\vec{w}}_t + \underline{\chi} \odot \vec{\boldsymbol{\mathcal{M}}}_{\mathcal{D}} \vec{\boldsymbol{\mathcal{L}}} [\underline{\vec{w}}_t] \right\|_{\mathcal{D}}^2}{\sum_t \left\| \underline{\chi} \odot \underline{\vec{E}}_t^{\text{inc}} \right\|_{\mathcal{D}}^2}. \quad (1)$$

For a transmitter t, $\underline{\vec{E}}_t^{\text{sct,meas}} \in \mathbb{C}^R$ is a vector of the measured scattered field at R receiver locations per transmitter located on the surface $\mathcal{S}$, $\underline{\chi} \in \mathbb{C}^I$ corresponds to a vector of the contrast values located at the triangle centroids in the domain $\mathcal{D}$, $\underline{\vec{w}}_t \in \mathbb{C}^I$ is a column vector that holds the contrast source values inside $\mathcal{D}$ and $\underline{\vec{E}}_t^{\text{inc}} \in \mathbb{C}^I$ holds the incident field vector values at the tetrahedra centroids in $\mathcal{D}$.

The operators $\vec{\boldsymbol{\mathcal{M}}}_{\mathcal{S}} \in \mathbb{C}^{R \times E}$ and $\vec{\boldsymbol{\mathcal{M}}}_{\mathcal{D}} \in \mathbb{C}^{I \times E}$ are interpolatory matrix operators that transform field values calculated along the mesh edges E to spatial-vector field values at either the location of the receivers R on $\mathcal{S}$ or at the centroids of

Fig. 1. Novel 3D microwave imaging system with nylon cylinder target.

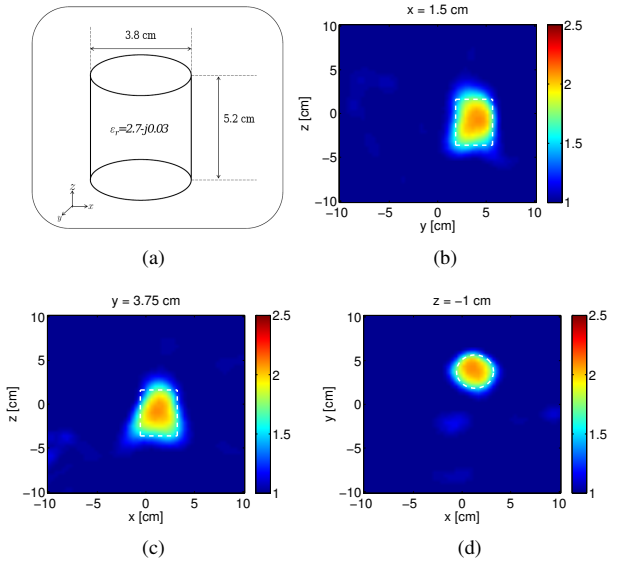

Fig. 2. (a) The first OI configuration, and 2D cross-section plots of the FEM-CSI reconstructions for 3.5 GHz at planes (b) x = 1.5 cm, (c) y = 3.75 cm and (d) z = -1 cm. The solid-white lines depict the expected location of the circular cylinder.

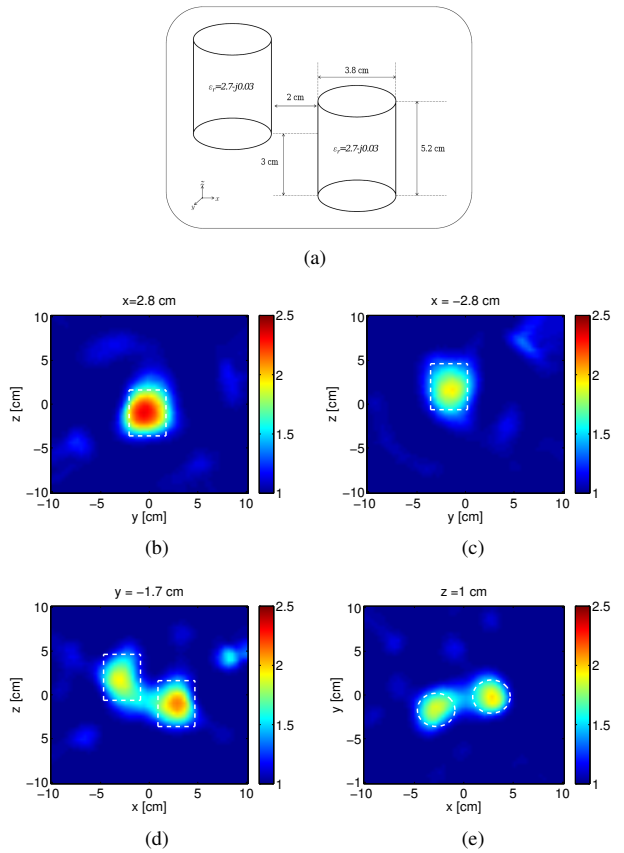

Fig. 3. (a) The second OI configuration, and 2D cross-section plots of the FEM-CSI reconstructions for 3.5 GHz at planes (b) x = 2.8 cm, (c) x = -2.8 cm, (d) y = -1.7 cm and (e) z = 1 cm. The solid-white lines depict the expected location of the circular cylinders.

the tetrahedra inside the imaging domain $\mathcal{D}$. The operator $\vec{\boldsymbol{\mathcal{L}}} \in \mathbb{C}^{E\times I}$ is the inverse FEM matrix operator [3]; it returns the scattered field values calculated along the mesh edges given the contrast source vector $\vec{w}_t$.

The FEM-CSI algorithm was implemented using C++ and parallelized utilizing the MPI library. The handling of sparse matrices and vectors, as well as computations involving them were done using PETSc [6]. The algorithm was run on a computer cluster consisting of 256 cores with 1 GB of physical memory available per core.

IV. Results and Conclusion

The FEM-CSI algorithm was used to invert the datasets for two OIs surrounded by air ($\epsilon_b = 1$). The first target is a nylon cylinder of circular cross-section with its center located at (1.5, 3.75, -1) cm. The radius and height of the cylinder are 3.8 cm and 5.25 cm respectively. The cylinder's dimensions and location with respect to transmitter one are depicted in Figure 2 (a). The relative permittivity of the nylon cylinder is $\epsilon_r = 2.7 - j0.03$. The second OI consists of two nylon cylinders, with their dimensions similar to the first target. The separation between the two cylinders is depicted in Figure 3 (a).

The datasets collected at a frequency of 3.5 GHz were inverted. For each dataset, the inversion algorithm was allowed to run for 300 iterations to ensure convergence. The imaging domain $\mathcal{D}$ was selected to be a sphere of radius 10 cm centered at the origin. The number of unknowns located inside the imaging domain was $\approx 157,000$ with the total number of tetrahedral elements in the mesh equal to $\approx 263,000$. With the algorithm running on 96 cores, the time per iteration was $\approx$ 20 seconds. The average memory utilized per core was 410 megabytes primarily devoted to store the inverse FEM operator.

The real part of the reconstructions is shown in Figures 2 and 3. The results are satisfactory, however the permittivity is under-estimated and artifacts appear in the images. This may be due to modeling error in terms of the incident field used by the algorithm and the assumed location and size of the calibration object.

References

[1] J. M. Geffrin and P. Sabouroux, "Continuing with the Fresnel database: experimental setup and improvements in 3D scattering measurements," *Inverse Probl.*, vol. 25, no. 2, p. 024001, Feb. 2009.

[2] M. Ostadrahimi, A. Zakaria, J. LoVetri, and L. Shafai, "A near-field dual polarized (TE-TM) microwave imaging system," *IEEE T. Microw. Theory*, 2013.

[3] A. Zakaria, "The finite-element contrast source inversion method for microwave imaging applications," Ph.D. dissertation, University of Manitoba, Mar. 2012.

[4] M. Asefi, M. Ostadrahimi, J. LoVetri, and L. Shafai, "Analysis of a 3D microwave imaging system," in *2013 IEEE Inter. Symp. on Antennas Propag. USNC-URSI Nat. Radio Science Meeting*, submitted July 2013.

[5] P. M. van den Berg and R. E. Kleinman, "A contrast source inversion method," *Inverse Probl.*, vol. 13, no. 6, pp. 1607–1620, Dec. 1997.

[6] S. Balay, J. Brown, K. Buschelman, W. D. Gropp, D. Kaushik, M. G. Knepley, L. C. McInnes, B. F. Smith, and H. Zhang, "PETSc Web page," 2012, http://www.mcs.anl.gov/petsc.